# Construction of a 3D Mooring Array of Temperature Sensors

HANS VAN HAREN, JOHAN VAN HEERWAARDEN, ROEL BAKKER, AND MARTIN LAAN

*Royal Netherlands Institute for Sea Research, Horntje, Texel, and Utrecht University, Utrecht, Netherlands*

(Manuscript received 12 May 2016, in final form 30 June 2016)

ABSTRACT

A small-scale 3D mooring array comprising up to 550 high-resolution temperature sensors was custom designed and constructed. The stand-alone array samples ocean temperature to depths of about 3000 m, limited by the buoyancy elements, at a rate of 1 Hz, with a precision better than 0.5 mK, a noise level better than 0.1 mK, and an endurance of 1 year. Its purpose serves quantitative studies on the development of turbulent mixing by internal wave breaking above deep-ocean topography. The 3D array consists of five parallel cables 105 m long with 3.2 mm inner diameter during the first deployment, now 5.5 mm. The cables are 4 and 5.6 m apart horizontally and are held under tension of 1000 N each using heavy buoyancy elements in a single line above. The entire array is folded into a 6-m high, 3-m-diameter structure above a 750-kg weight. It is deployed in a single overboard operation similar to that of a free-falling mooring. New here is the unfolding of the compacted array when hanging overboard and prior to release into free fall.

## 1. Introduction

The global oceans contain a wide variety of motions at scales varying from millimeters (turbulence dissipation) to thousands of kilometers (basin circulation). The latter are mainly two-dimensional (2D) horizontally spatial. The former however are spatially fully 3D and are essential for the redistribution of materials and energy. Like in the atmosphere, life would come to a halt without turbulence: breathing and feeding are virtually impossible without it even for the smallest organisms that live in a laminar microscopic world. In the ocean interior outside the surface wave influence, most turbulence is generated via the breaking of internal waves above sloping bottoms of underwater topography (e.g., Eriksen 1982; Thorpe 1987). Because of severe limitations of the harsh ocean conditions imposed by salinity, pressure, and waves, measurements on internal wave turbulence dynamics are few and far between, and much is still to be learned about the relevant processes that dominate diapycnal (vertical) turbulent exchange.

Quantitatively, ocean turbulence dissipation has been mainly estimated using shipborne 1D vertical 100-Hz sampling rate microstructure profiling measuring shear variations measuring the smallest details (e.g., Oakey 1982; Gregg 1989), and a 10–20-Hz sampling rate CTD profiling measuring the largest turbulent energy containing overturn sizes of unstable density portions (Thorpe 1977). More recently, overturn sizes have been estimated using 1D moored thermistor strings, of 10–20-m vertical separation at a 0.01-Hz sampling rate (Levine and Boyd 2006; Aucan et al. 2006) and of 1-m vertical interval separation at a 1-Hz sampling rate equipped with high-resolution temperature sensors (van Haren and Gostiaux 2012). Thus far, 3D quasi-turbulence measurements were difficult to make in the ocean due to logistic problems.

This is in spite of exciting mooring experiments on open ocean internal wave correlation using conventional (nonturbulence) instrumentation in the 1970s. Pinkel (1975) used three booms of about 20-m length from the Research Platform *Floating Instrument Platform* (*FLIP*) to simultaneously move temperature and pressure instruments 190 m up and down, once every 100–150 s. The *FLIP* resolved horizontal scales of about 40 m and vertical scales of about 1 m. The Internal Wave Experiment (IWEX) consisted of a large pyramid of deep-sea mooring lines equipped with 10–15-min-sampling-rate current meters and temperature sensors in the open west Atlantic Ocean (Briscoe 1975). The IWEX resolved scales between 6 and 3000 m. From these experiments, and another more conventional deep-sea

*Corresponding author address*: Hans van Haren, Royal Netherlands Institute for Sea Research, P.O. Box 59, 1790 AB Den Burg, Texel, Netherlands.
E-mail: hans.van.haren@nioz.nl

DOI: 10.1175/JTECH-D-16-0078.1

multiple mooring experiment (Saunders 1983), it is known that all but the largest internal waves at near-inertial and tidal frequencies decorrelate at horizontal scales of about 1000 m (Briscoe 1975; Saunders 1983; van Haren 2004). The IWEX and *FLIP* experiments showed much higher correlation in the internal wave band, but even at the 6-m horizontal scale the coherence was becoming well less than one (nonsignificant) upon approaching the buoyancy frequency. At scales $O(10)$ m and $O(100)$ s, the buoyancy frequency separates internal waves at lower frequencies from turbulence at higher frequencies, with the inertial subrange being poorly resolved.

Observations from the acoustic Doppler current profiler (ADCP)'s four slanted beams sampled at 2 Hz halfway up the continental slope in the Bay of Biscay confirmed these (de)correlation scales for highly nonlinear turbulent bores that dominate internal wave breaking above the sloping topography (van Haren 2007). The 20° beam angle from the vertical acoustic caused a spread of 30 m, on average, over an 80-m range, which demonstrated considerable deformation patterns in acoustic reflection amplitude in each of the four beams.

However, an ADCP is a primitive means of 3D sampling. Although it is capable of establishing particle and phase/propagation speed, it has two disadvantages. First, the ADCP's slanted beams deform the signal of the passing structure as it is sampled at different time intervals in the vertical between opposing beams. Second, single-frequency acoustic devices like an ADCP provide echo intensity data that are basically impossible to quantify in terms of turbulence characteristics. More quantitative measurements can be made using high-resolution temperature sensors, but free-falling moorings cannot be dropped at a precision better than about 100 m horizontally in the deep sea (unpublished attempts by our team).

Alternatively, one could lower the mooring lines via a winch cable several thousands of meters to the bottom. Hereby, a precision of a few meters horizontally can be obtained only by using a long-baseline acoustic positioning system, to be deployed first. This is an expensive additional operation, performed only for an extensive set of moorings, like for an underwater neutrino telescope such as the Astronomy with a Neutrino Telescope and Abyss Environmental Research (ANTARES) off Toulon, France (Ageron et al. 2011). The present ANTARES mooring line separation is 90 m on average, which exceeds the required horizontal decorrelation scale resolution for internal waves by one order of magnitude if one wants to resolve the internal wave–turbulence transition (Pinkel 1975; Briscoe 1975; Thorpe 2010). Thus, in order to resolve the internal wave–turbulence phenomena in some detail, the only solution seems to be to deploy multiple mooring lines in a single structure, somewhat like IWEX.

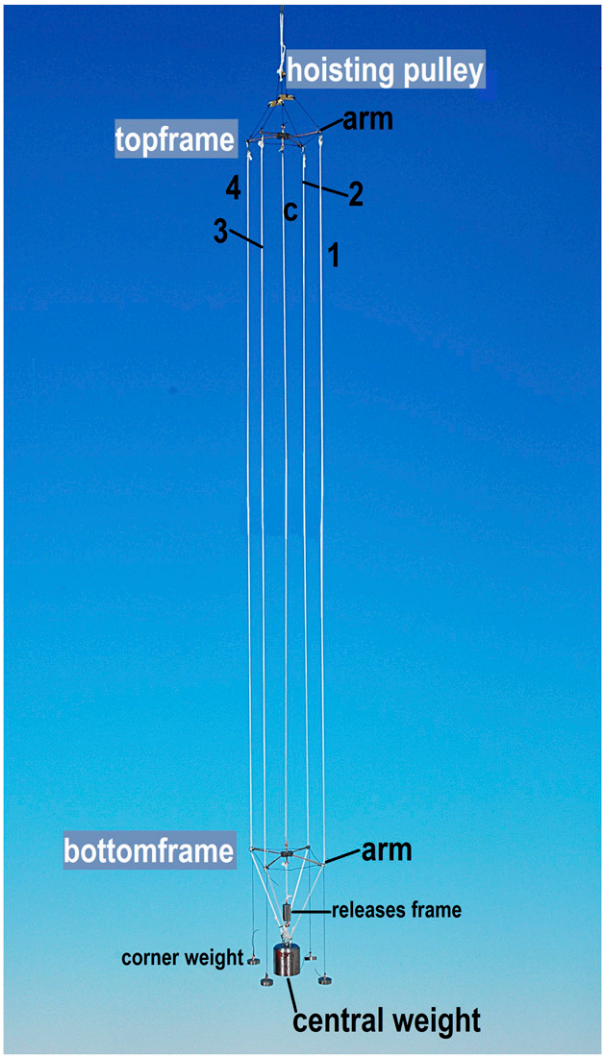


FIG. 1. First model of the 3D five-line mooring array, to scale.

In contrast to the multiscale pyramid form in IWEX and the slanted beams of an ADCP, we chose to design a multiparallel-cable array with the requirements to resolve 1-m vertical scales over a range of 100 m and <10-m horizontal scales. This is similar to that proposed by Thorpe (2010) for a freely drifting device. Our dimensions are larger, especially in the vertical, by a factor of 10, and we prefer to have a moorable system to avoid Doppler shift in frequency (Gerkema et al. 2013). As such a system is not usually deployable from a ship, a further requirement is to compact the entire array before overboard operation and to unfold it before dropping it into the ocean to descend to the seafloor. In

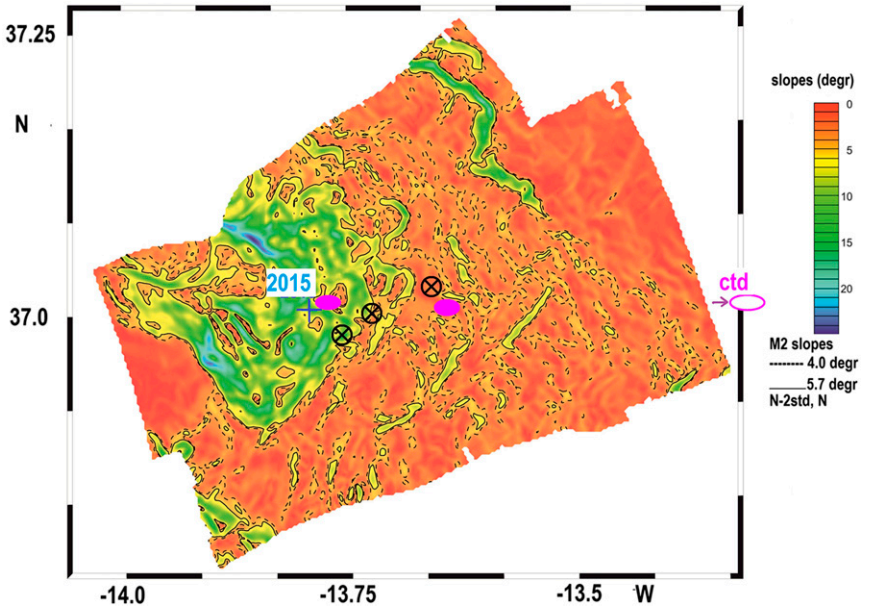


FIG. 2. Mooring area to the east of the southern subsummit (37°02′N, 13°58′W) of the Josephine Seamount. The present site (blue) is shallower than three previous ones (black circle with cross) deployed in 2012–13 (van Haren et al. 2015). Nearby and far CTD stations are indicated by purple ellipses, one outside the page. Critical $M_2$ internal tidal slopes are computed for mean (N, solid line) and weak stratification (N-2 standard deviations, dashed line).

this paper, we describe technical details of this ''small scale'' 3D mooring array of temperature sensors.

## 2. Technical details

### *a. 3D mooring array of temperature sensors*

At the Royal Netherlands Institute for Sea Research [Nederlands Instituut voor Onderzoek der Zee (NIOZ)], a 6-m tall, 3-m-diameter folding high-grade aluminum structure has been designed and built. It consists of two support frames of 1.7 m × 1.7 m each holding a set of four arms 3.3 m long (Fig. 1). At the lower arms and on the lower support frame, a maximum of 520 NIOZ4 high-resolution temperature sensors can be held in tubes that are taped at 1.0-m (vertical) intervals to the original five 105-m-long nylon-coated steel cables and stored in plastic electrician's cable gutters. During the first deployment described here, the cables had a 3.2-mm inner diameter [ID; 3.6-mm outer diameter (OD)] of 8600-N breaking strength. Because of corrosion problems as a result of bad coating, this cable needs to be replaced. Four instrumented cables connect the corner tips of the upper and lower sets of frame arms (corner cables 1–4); a central instrumented cable connects the upper and lower inner frames (central cable c). The corner cables are horizontally separated by 4.0 m from the central cable, and 5.6 (or 8) m between each other. At the tips of the eight arms and along the 4.2-m vertical cables from the tips of the lower arms to four 25-kg bottom weights, additional NIOZ4 sensors can be mounted that are programmed to also register acceleration (tilt) and compass data along three axes. NIOZ4 are self-contained temperature sensors sampling at a rate of 1 Hz with a battery and memory capacity for over one year, with a precision better than $5 \times 10^{-4}$ °C and a noise level of 0.5–1 $\times 10^{-4}$ °C—the latter depending on the programmed measurement interval of the Wien bridge oscillator. Every 4 h, all sensors on a mooring, here ~500, are synchronized via induction to a single standard clock, so that times are <0.02 s off. This requires nylon-coated cables to insulate the steel from the salty environment, using the latter for the return to close the current loop. For further details, see van Haren et al. (2001, 2009) on NIOZ4's predecessors with similar characteristics.

To provide rigidness to the mooring array, the support frames are interconnected in several ways and tension is distributed across all the cables. The lower support frame is connected directly and via four slanted support cables to a near-bottom ''release frame'' with two acoustic releases holding the 750-kg central bottom weight (Fig. 1). The four arm tips are also interconnected via horizontal cables. Chains of 0.2 m in diameter prevent the arms from

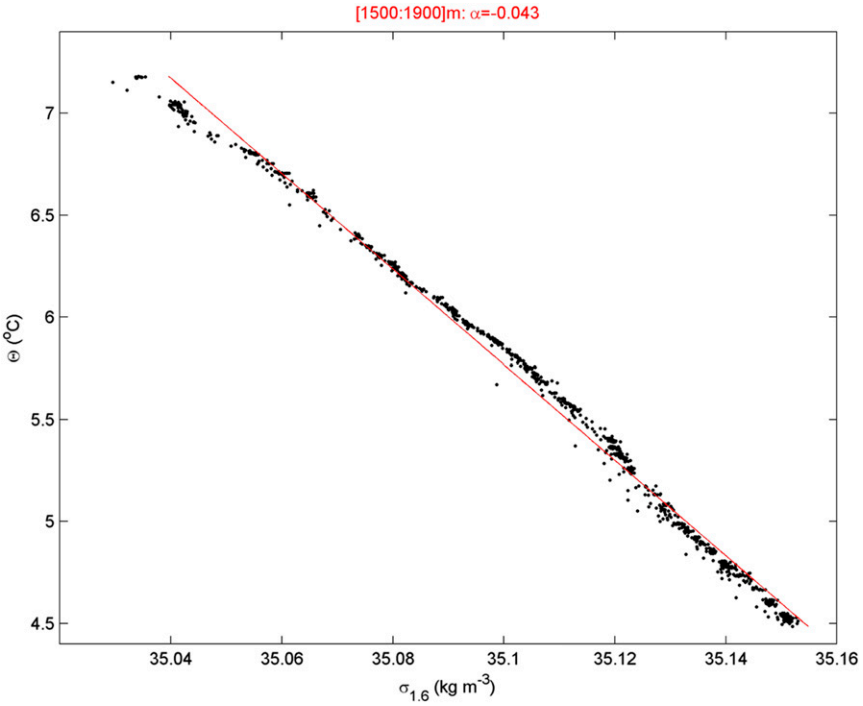


FIG. 3. Conservative temperature–density anomaly referenced to 1600 m from nearby CTD observations one day after mooring deployment for a ±200-m range around the 3D mooring array water depth. The best-fit linear relationship is given by the straight red line: $\delta\sigma_{1.6} = \alpha\delta\Theta$; $\alpha = -0.043 \pm 0.002\ \mathrm{kg\,m^{-3}\,K^{-1}}$ is the apparent local expansion coefficient.

overstretching. Similar support and interconnection cables and chains are attached to the upper support frame. The slanted cables connect via an aluminum connection tube to a single nylon-coated mooring cable (5.5-mm ID steel; 6.3-mm OD; 19 000-N breaking strength) and to the (elliptic) buoyancy elements ("top buoys") above. Depending on the number of top buoys used, the single mooring cable is 100–200 m long. A small compressible float is attached to prevent the connection tube from falling onto the upper support frame during the first meters of free-fall drop. The top buoys distribute a net buoyancy of about 5000 N over the five instrumented cables, so as to have a 1000-N net buoyancy per cable and sufficient tension-torque to keep the structure rigid under water at moderate current speeds (roughly $<0.3\,\mathrm{m\,s^{-1}}$). The tension–torque, the elliptic buoyancy, the thin cables, and the open structure of the arms have been designed for minimum mooring motion upon current drag. During deployment prior to release, approximately the same tension (~6000 N) is built up by the bottom weight. The thin instrumented cables stretch approximately 0.17 m over their full length under 1000-N tension, so that they effectively act as balancers in case of uneven distribution of the tension.

Next to the central instrumented cable, an 8-mm-diameter Dyneema line (with 62 000-N breaking strength) is used to lower the central weight whereby the two sets of four arms are unfolded and the sensors are pulled out of the gutters. This line is also used to fold up the entire mooring upon recovery, and it serves as a backup should the instrumented cables break.

### b. *Mooring site and conditions*

The 3D mooring array of temperature $T$ sensors was successfully moored for the first time at 37°00′N, 013°49′W, at 1740-m water depth on the eastern flank of the Josephine Seamount, about 400 km southwest of Lisbon, Portugal, in the northeastern Atlantic Ocean (Fig. 2) on 2 May 2015 (yearday 121). It was recovered on 17 August 2015. For the present configuration, we taped a total of 487 NIOZ4 sensors to the 3D array, with 95 sensors to each of the five cables, eight sensors at the arm tips, and four sensors to a single bottom-weight line, with the lowest sensor approximately at 1 m from the bottom. Although the mooring could hold acoustic current devices, it was decided to mount these in a separate mooring nearby to avoid bad data due to reflections off the many $T$ sensors in the 3D array. The average local bottom slope is about 10°, which is twice steeper, "supercritical," than the average slope of internal tides under local stratification conditions (van Haren et al. 2015).

FIG. 4. Compacted mooring array buildup with all upper arms and one lower arm mounted, in its custom-made horizontal position support; quay side of Ponta Delgada (Azores, Portugal), after container transport and prior to research vessel arrival.

The site is also well below the Mediterranean Sea outflow, which is located between 1000 and 1400 m here, so that salinity-compensated apparent density inversions in temperature are expected to be minimal. Knowledge about the local temperature–density relationship is important for using moored $T$ data as a tracer for density variations to be able to estimate turbulence parameters.

After the application of laboratory calibration and correction for drift, the $T$ data are converted into "conservative" (potential) temperature $\Theta$ (IOC 2010). They are used as a tracer for density anomaly ($\sigma_{1.6}$, referenced to 1600 m) variations following the relation $\delta\sigma_{1.6} = \alpha\delta\Theta$, $\alpha = -0.043 \pm 0.002\,\mathrm{kg\,m^{-3}\,K^{-1}}$, where $\alpha$ denotes the apparent thermal expansion coefficient under local conditions. This relation is established from nearby shipborne conductivity–temperature-depth (CTD) profile data (Fig. 3). The number of $T$ sensors and their spacing of 1.0 m, in combination with their low noise level, allow for estimating turbulence parameters like dissipation rate $\varepsilon$ and, under particular assumptions for mixing efficiency, vertical eddy diffusivity via the reordering of unstable overturns make every 1-Hz sampled "density" profile a static stable one (Thorpe 1977). As in Thorpe (1977, 1987), a constant factor of 0.8 is used relating thee displacement scales following the reordering to Ozmidov scales, the largest scales of stratified turbulence. The buoyancy frequency is computed from the reordered density ($T$) profiles, and a constant mixing efficiency of 0.2

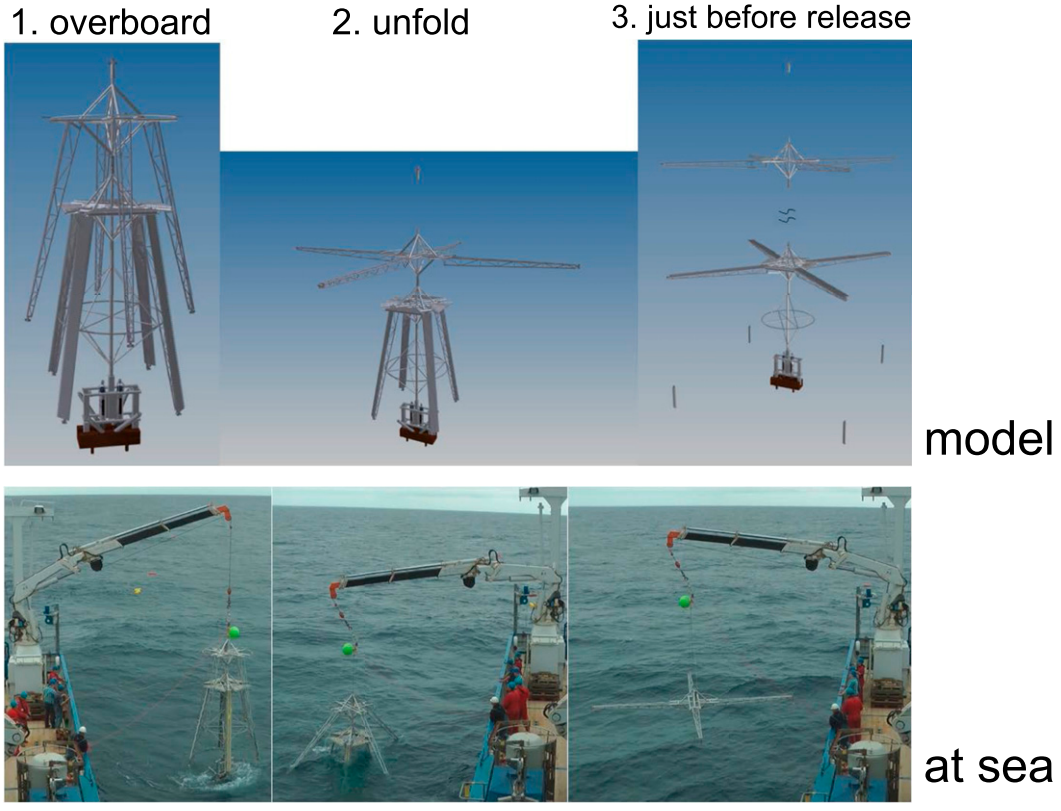


FIG. 5. Schematic of the principal steps in overboard unfolding of the 3D mooring array. (upper right) Note that the vertical distance in the model just before release is not to scale.

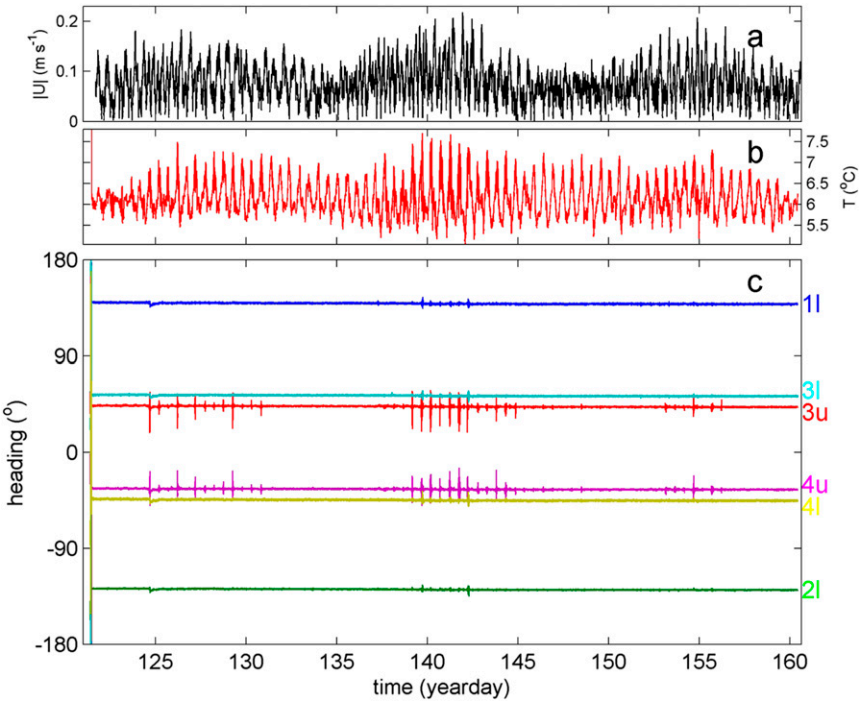


FIG. 6. Thirty-eight days of observations between deployment on day 121.5 and cable 4 breaking on day 160.4. (a) Current speed measured at a mooring 1.1 km away; average for the range [−1840, −1640] m. (b) Temperature measured at the upper arm tip above cable 4. (c) Heading from six compass sensors at four lower (l) arm tips and two upper (u) arm tips. Corner cable numbers are indicated.

is used to compute diffusivity. Further details of this method for moored thermistor sensor data are in van Haren and Gostiaux (2012). Here, vertical averaging is denoted by ⟨⟩, while time averaging is denoted by [ ].

## 3. Overboard operations

### a. Preparation

The entire aluminum structure, including buoyancy elements and bottom weight, fits into a standard 20-ft sea container for easy transportation. To prevent long periods of void data during transportation, the compacted 3D mooring array is best built up in the port of departure prior to the deployment cruise. This is done in the horizontal position using two custom-made supports (Fig. 4). After programming all temperature sensors in one operation (van Haren et al. 2009), they are put into plastic tubes that are pretaped to the instrument cables. The arms of the lower frame are filled with sensors by clicking the tubes into the gutters. Hereby, the cable hangs loosely out at the gutters' sides. The central cable follows a complex packing scheme for filling its gutters on the inner portion of the lower frame. The upper and lower frames are put on the horizontal position supports and connected, displaced by 45° with respect to each other for compacting, whereby two release pins secure their connection and prevent, with additional band clamps, the arms from unfolding.

After mounting the arms to the upper and lower frames and securing them, support and interconnection cables are held in position by elastic bands. The Dyneema line is inserted through the central pipe before putting the structure upright in the near-bottom release container above the bottom weight. On deck just prior to deployment, a small (~150-N buoyancy) compressible float, the single mooring cable (to be connected to the mooring's top buoys), and the crane for lifting the entire compacted mooring array are attached to the upper frame tube via a quick-release hook immediately under a hoisting pulley. The Dyneema line is put through a ring and through the pulley to a winch. The two-release-pin lines, the quick-release line, the mooring cable, and the line holding the ring to recover the Dyneema line are all put on one side of the structure.

### b. Deployment

A video of the deployment is available online (at https://youtu.be/C2DizkNW2dM).

After putting the mooring top buoys overboard from the stern and stretching the cables between them, the

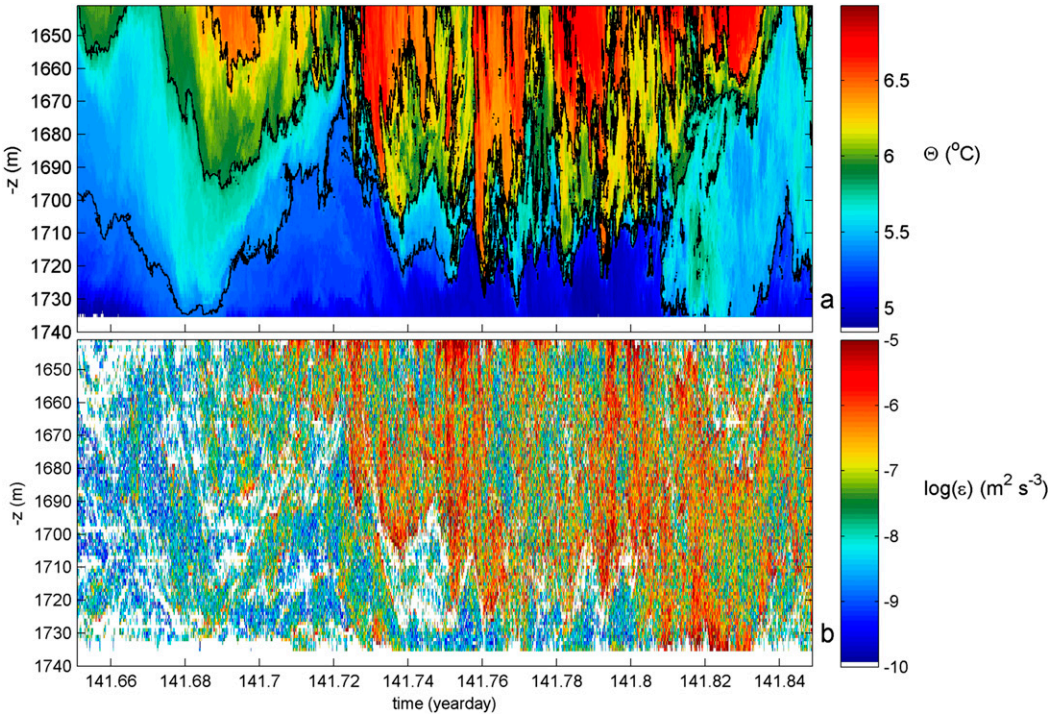


FIG. 7. Full vertical range and 17 300-s (~4.8 h) depth–time images of multiple large overturning from above observed at the central cable. (a) Conservative temperature, with isotherms contoured at 0.5°C intervals. (b) Logarithm of dissipation rate.

forward motion of the ship is reduced to a minimum. The band clamps securing the arms are removed and the 1200-kg compacted 3D mooring array is lifted over the side (Fig. 5, left). The weight is immediately put into the water to dampen the swaying. The Dyneema line is hoisted to lift the bottom weight in order to be able to release the upper frame's security pin. Just before the upper arms are folded out (Fig. 5, middle), the lower frame's security pin is released. The complete structure is free now, and the upper arms rotate 45° to be placed directly above their corresponding underarm. The Dyneema line is veered as rapidly as possible to build up some tension in the five instrumented cables. Just before completing the unfolding, full (~6000 N) tension is transferred from the weight-lowering Dyneema line to the five thin steel cables. The structure settles into mooring mode. The now tensionless Dyneema line, with a slight overlength of 0.2 m compared to the five cables, is pulled aboard using the ring line and is taped to the single mooring cable (leading to the top buoys). The frame is lowered further into the water by the crane, prior to the free-fall release.

### c. *Recovery*

The recovery of the 3D thermistor array is by and large not much different from a standard 1D ocean mooring. Upon release of the bottom weight, the pickup line and heavy top buoy arrive at the surface. After pickup via manoeuvring the ship alongside the array, the single mooring cable is spooled up a winch while removing the buoyancy elements. When the Dyneema line is reached, spooling of the cable stops. The Dyneema line is untaped from the cable, put through the pulley onto a small winch, and the crane hook with a pulley are attached to the mooring cable.

The Dyneema line is slowly spooled whereby the 3D mooring array is folded up more or less to its compacted form while still being below the keel of the ship. After completion of folding, the compacted array is hoisted aboard. All instrumented cables hang in loops under the compacted array. They are pulled aboard by hand. The sensors are removed from their plastic tubing; the tubes remain fixed to the mooring cables for reuse. The sensors are opened one by one, the Secure Digital (SD) card is read and the battery is refreshed before revacuuming.

## 4. First results

Under favorable weather conditions (4–7 m $s^{-1}$ wind speeds and 1–2-m waves), the mechanical overboard deployment operation went as planned. Three-and-a-half months later, the recovery procedure also went smoothly, but four instrumented cables turned out to be

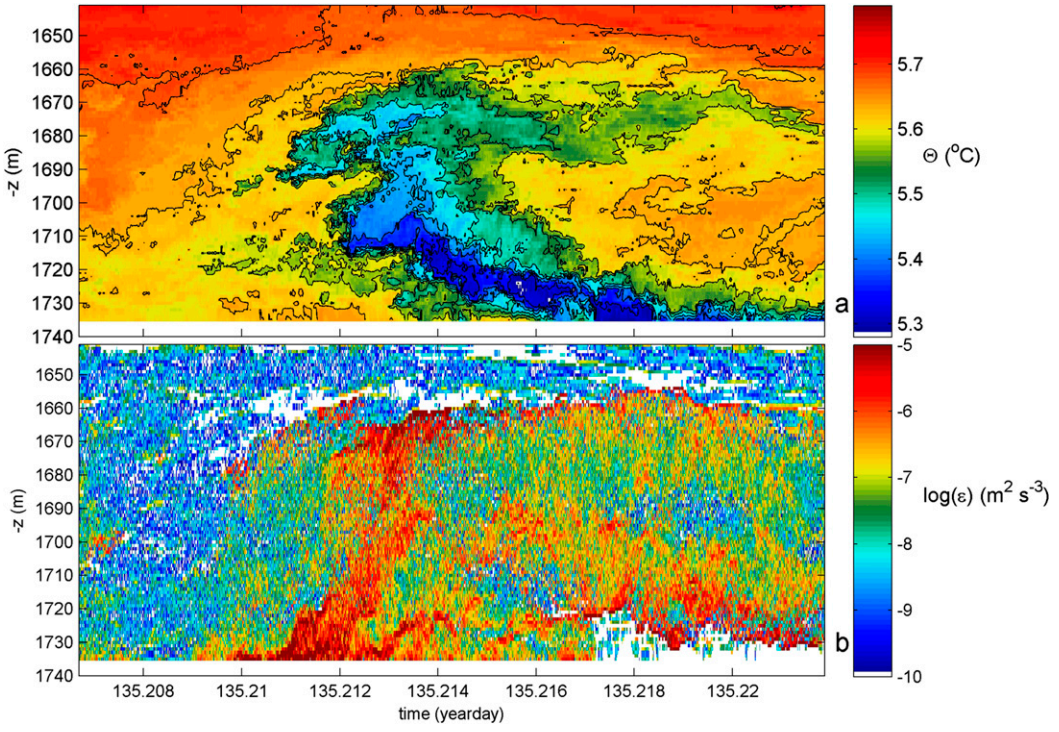


FIG. 8. As in Fig. 7, but for 1300 s (~0.3 h) of a single large overturning and upslope-propagating nonlinear bore. Note the different temperature range in (a); here with isotherms contoured at 0.05°C intervals.

broken and five sensors were lost. A galvanic corrosion problem due to poor coating caused three long cables and the single instrumented short bottom-weight cable to break within a week of each other, the first (cable 4) after 38 days under water. The corrosion was not associated with an oceanographic event and the failure of one of the cables did not cause others to break. In spite of the corrosion problem, nearly all sensors could be recovered, because none of the cables broke at more than one spot. Of the eight sensors on the tips of all arms that registered compass data and acceleration besides temperature, two failed (upper-arm tips of cables 1 and 2). Besides these 2 sensors and the 5 sensors that were lost, 32 sensors failed either mechanically or electronically. This amounts to an overall data loss of about 8%; temperatures at these positions are interpolated.

The first 38 days of all cables under tension showed good data. The mooring did not considerably move under the maximum 0.22 m s$^{-1}$ current speeds (Fig. 6). Although we have only current information (Fig. 6a; 200 m vertically averaged data) from a simultaneous mooring located 1.1 km off slope, which can cause some phase difference in motions, the arm tip's heading information (Fig. 6c) seems be related more to temperature (Fig. 6b). In general, after the deployment on day 121.5, all six working compasses showed very little variation (±0.2°) around their mean values. Between the different arm tips, the mean values were off by multiples of 90° to within ±8° error. This error is caused by imperfect calibration, which was done at the dike outside our laboratory, or due to a slight offset in mounting, which was done by eye.

Occasionally, and related to the warm temperatures occurring at the semidiurnal tidal periodicity mainly, short-term (e.g., on day 141.8) heading variations of ±10° occurred on the upper arms (red and purple) and ±1° on the lower arms. These high-frequency "mooring vibrations" were caused by relatively strong turbulent motions, mainly coming from above. They are not associated with larger-scale approximately horizontal currents. An example is given in some detail in Fig. 7. Noting the vertical range of almost 100 m above the bottom, short (~500 s) fluctuations of alternating warm and cooler waters are seen to be moved up and down over three-quarters of the range (Fig. 7a). The time of variation is much shorter than the local mean buoyancy period of about 3500 s (~1 h) and thus represents turbulent overturning, in this case mainly convectively driven. The depth–time mean dissipation rate equals $\langle[\varepsilon]\rangle = 1.1 \pm 0.5 \times 10^{-6}\,\mathrm{m^2\,s^{-3}}$ for the image in Fig. 7b. The standard deviation mainly reflects errors in the method. The variation in estimates from all five cables amounts only $\pm 0.2 \times 10^{-6}\,\mathrm{m^2\,s^{-3}}$. We note that the cables are equipped with completely independent sensors.

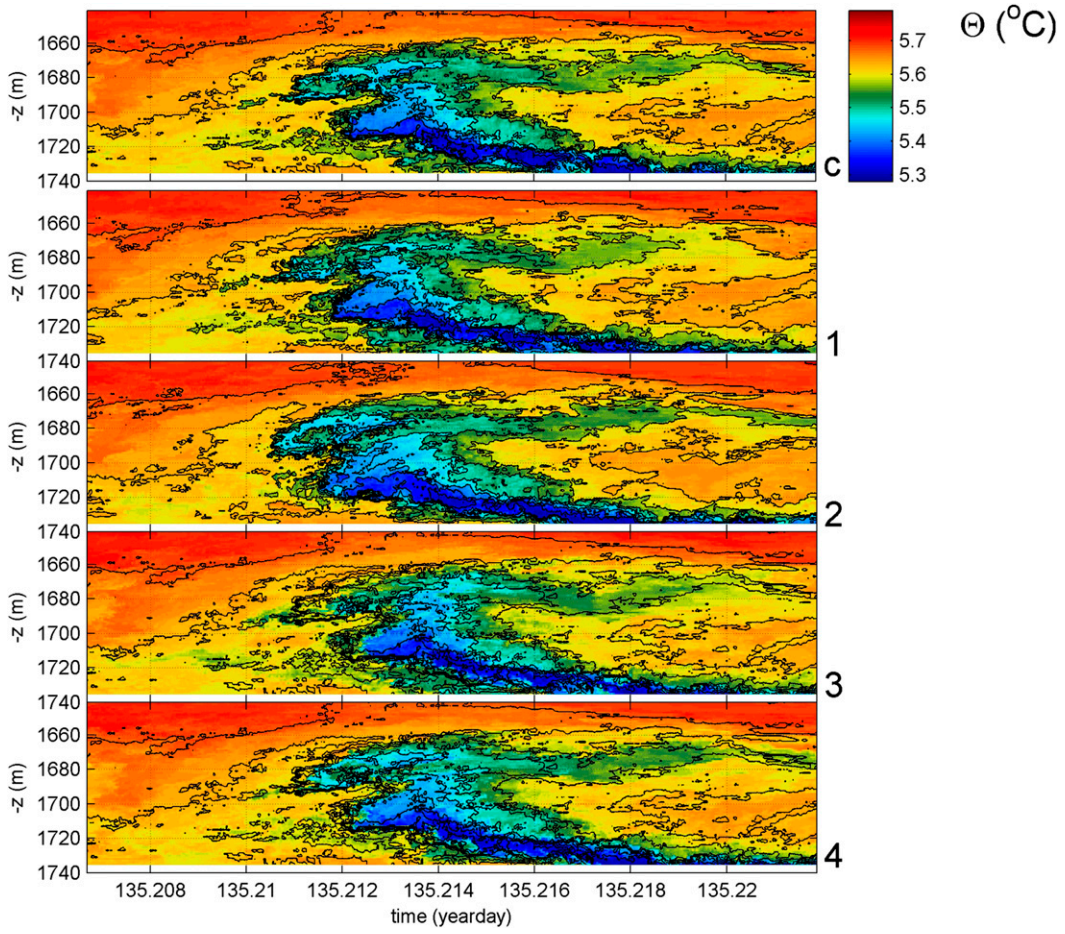


FIG. 9. Single large overturning bore from Fig. 8. Temperature observed at all five cables (corner cables 1–4 and central cable c).

An example of shear-driven turbulence is given in Fig. 8. Although the mean buoyancy is about 1.5 times less than for the previous example for the given $T$–density relationship, the turbulence dissipation rate is still $\langle[\varepsilon]\rangle = 0.7 \pm 0.4 \times 10^{-6}\,\mathrm{m^2\,s^{-3}}$ due to the large overturning including (smaller) overturns working against the small-scale stratified layers. The bottom-related single 70-m-tall overturn is associated with the upslope motion of cold water after the turn of the tide. This borelike motion of a highly nonlinear wave is a well-known phenomenon of near-bottom turbulence generation and is important for sediment resuspension above sloping topography (Hosegood et al. 2004). In contrast to the convective turbulence generated from above in Fig. 7, the nonlinear bore hardly affects the mooring by vibrations, as the heading remains quiescent around day 135 (Fig. 6c).

The single frontal bore is instructive for a turbulence development inspection between the five instrumented cables (Fig. 9). It is seen that both the first front (around day 135.212) and the secondary overturned front (around day 135.216) appear first at cables 1 and 2 before the central cable and cables 3 and 4. In between, smaller overturns may show different development and order of appearance.

Although the image in Fig. 9 does not show distinctive differences at first glance, the computation of temperature differences referenced to those from the central cable shows a much more varied picture of the occurrence and size of incoherent patches (Fig. 10). The upper panel of Fig. 9 is repeated here for reference. The differences in the lower four panels exceed 0.1°C (in absolute value). The larger patches typically last 40 s and extend 10–20 m. Depending on the direction of the current with respect to the mooring orientation, early arrival of a cold front and late arrival of a warm front may show as blue (cooler), with respect to the central cable. Thus, the first cold front shows as blue (cooler) in Figs. 10(1-c) and 10(2-c), and as red (warmer) in Figs. 10(3-c) and 10(4-c). The secondary overturned front shows

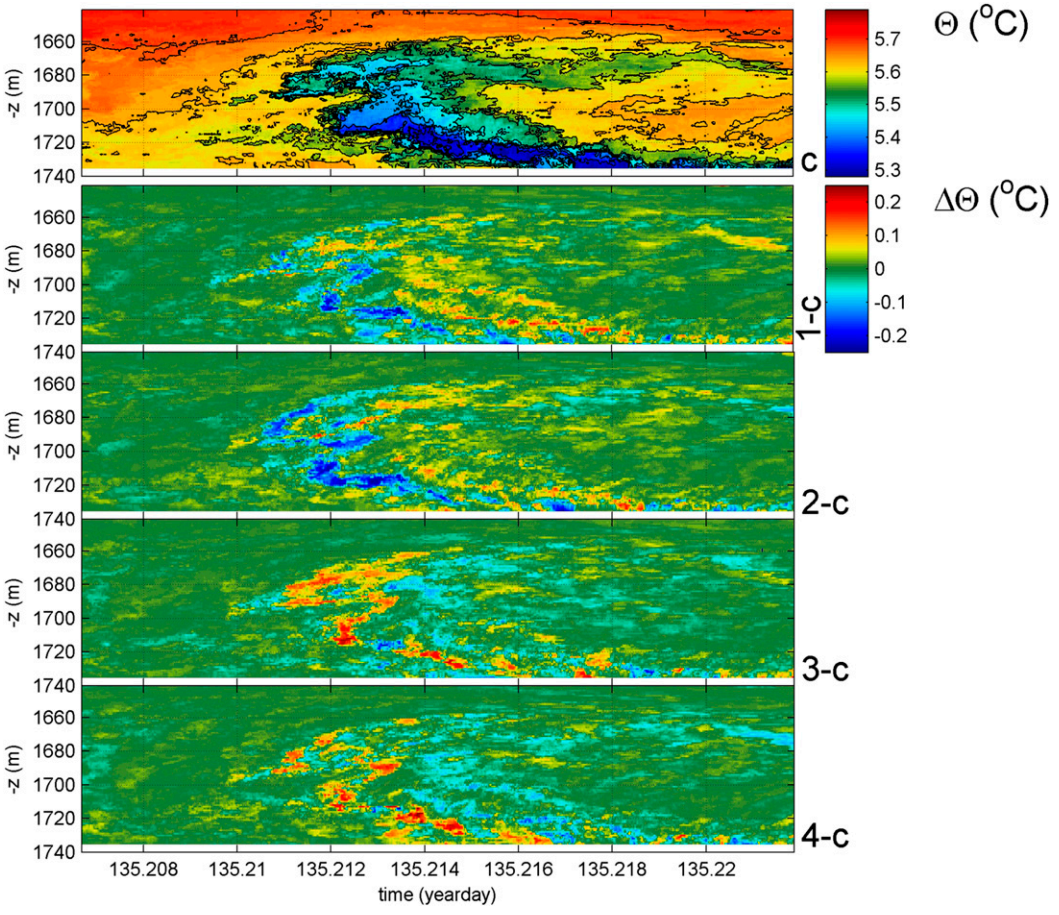


FIG. 10. As in Fig. 9, but for central cable c and its temperature difference with all four corner cables computed for all 95 sensor position levels.

more incoherently colored patches, informing that regular turbulent patches are created during the passage between the lines.

## 5. Conclusions

We have successfully deployed a multi-instrumented, multicable 3D mooring array of temperature sensors, in the fashion of a single free-fall mooring operation. The expected tension became well distributed over the cables, and the torque was sufficient to provide a stiff mooring, for a drag imposed by maximum $0.22\,\mathrm{m\,s^{-1}}$ current speeds. With respect to a single-line 1D mooring, the rotation of the cables was much less than for a vibrating cable with swiveled instruments in between (van Haren 2010). The heading of the present five-cable mooring was only distorted by on average ±5° when (its top was) subjected to vigorous convective overturning from above.

For ocean turbulence studies on the relatively small scale of 1–10 m, the size of the array seems adequate, in combination with the 1-Hz sampling rate and ~0.1-mK noise level of the high-resolution temperature sensors. Future detailed investigations seem possible to reveal the development of nonlinear turbulent bores and convective overturning. Naturally, it is desirable to resolve the entire scale range from turbulence dissipation ($10^{-3}$ m) to the largest internal waves ($10^{3}$ m), but that is simply not feasible with a single deployable mooring array.

For future deployments we have to replace the thin instrumented cables with our ''standard'' mooring cables (5.5-mm ID; 6.3-mm OD; 19 000-N breaking strength), which have a superior coating. The disadvantages are less stretch under given tension, some more drag, and additional 30-kg weight, and thus some extra buoyancy is needed. However, it will solve the galvanic corrosion problem experienced during this first deployment, as historic 1D moorings of temperature sensors, using the same cable and the same synchronization principle, never caused any corrosion problem previously, not even after 1.5 years of underwater time. Thus, the mechanical structure will last as long as the battery capacity of the sensors.

*Acknowledgments.* This research was supported in part by NWO, the Netherlands Organization for the Advancement of Science. We thank the captain and crew of the R/V *Pelagia* and M. Bakker of MTM at NIOZ for their very helpful assistance during deployment and recovery. J. Blom and J.-D. de Visser assisted during construction projects.

## REFERENCES

Ageron, M., and Coauthors, 2011: ANTARES: The first undersea neutrino telescope. *Nucl. Instrum. Methods Phys. Res.*, **656A**, 11–38, doi:10.1016/j.nima.2011.06.103.

Aucan, J., M. A. Merrifield, D. S. Luther, and P. Flament, 2006: Tidal mixing events on the deep flanks of Kaena Ridge, Hawaii. *J. Phys. Oceanogr.*, **36**, 1202–1219, doi:10.1175/JPO2888.1.

Briscoe, M. G., 1975: Preliminary results from the trimoored internal wave experiment (IWEX). *J. Geophys. Res.*, **80**, 3872–3884, doi:10.1029/JC080i027p03872.

Eriksen, C. C., 1982: Observations of internal wave reflection off sloping bottoms. *J. Geophys. Res.*, **87**, 525–538, doi:10.1029/JC087iC01p00525.

Gerkema, T., L. R. M. Maas, and H. van Haren, 2013: A note on the role of mean flows in Doppler-shifted frequencies. *J. Phys. Oceanogr.*, **43**, 432–441, doi:10.1175/JPO-D-12-090.1.

Gregg, M. C., 1989: Scaling turbulent dissipation in the thermocline. *J. Geophys. Res.*, **94**, 9686–9698, doi:10.1029/JC094iC07p09686.

Hosegood, P., J. Bonnin, and H. van Haren, 2004: Solibore-induced sediment resuspension in the Faeroe-Shetland Channel. *Geophys. Res. Lett.*, **31**, L09301, doi:10.1029/2004GL019544.

IOC, 2010: The international thermodynamic equation of seawater—2010: Calculation and use of thermodynamic properties. Intergovernmental Oceanographic Commission Manuals and Guides 56, UNESCO, 207 pp.

Levine, M., and T. J. Boyd, 2006: Tidally forced internal waves and overturns observed on slope: Results from HOME. *J. Phys. Oceanogr.*, **36**, 1184–1201, doi:10.1175/JPO2887.1.

Oakey, N. S., 1982: Determination of the rate of dissipation of turbulent energy from simultaneous temperature and velocity shear microstructure measurements. *J. Phys. Oceanogr.*, **12**, 256–271, doi:10.1175/1520-0485(1982)012<0256:DOTROD>2.0.CO;2.

Pinkel, R., 1975: Upper ocean internal wave observations from Flip. *J. Geophys. Res.*, **80**, 3892–3910, doi:10.1029/JC080i027p03892.

Saunders, P. M., 1983: Benthic observations on the Madeira Abyssal Plain: Currents and dispersion. *J. Phys. Oceanogr.*, **13**, 1416–1429, doi:10.1175/1520-0485(1983)013<1416:BOOTMA>2.0.CO;2.

Thorpe, S. A., 1977: Turbulence and mixing in a Scottish loch. *Philos. Trans. Roy. Soc. London*, **286A**, 125–181, doi:10.1098/rsta.1977.0112.

——, 1987: Transitional phenomena and the development of turbulence in stratified fluids: A review. *J. Geophys. Res.*, **92**, 5231–5248, doi:10.1029/JC092iC05p05231.

——, 2010: Breaking internal waves and turbulence dissipation. *J. Mar. Res.*, **68**, 851–880, doi:10.1357/002224010796673876.

van Haren, H., 2004: Spatial variability of deep-ocean motions above an abyssal plain. *J. Geophys. Res.*, **109**, C12014, doi:10.1029/2004JC002558.

——, 2007: Echo intensity data as a directional antenna for observing processes above sloping ocean bottoms. *Ocean Dyn.*, **57**, 135–149, doi:10.1007/s10236-006-0095-9.

——, 2010: Rapid swing and spin of [deep] taut-wire-moored instruments. *Deep-Sea Res. I*, **57**, 909–917, doi:10.1016/j.dsr.2010.04.007.

——, and L. Gostiaux, 2012: Detailed internal wave mixing observed above a deep-ocean slope. *J. Mar. Res.*, **70**, 173–197, doi:10.1357/002224012800502363.

——, R. Groenewegen, M. Laan, and B. Koster, 2001: A fast and accurate thermistor string. *J. Atmos. Oceanic Technol.*, **18**, 256–265, doi:10.1175/1520-0426(2001)018<0256:AFAATS>2.0.CO;2.

——, M. Laan, D.-J. Buijsman, L. Gostiaux, M. G. Smit, and E. Keijzer, 2009: NIOZ3: Independent temperature sensors sampling yearlong data at a rate of 1 Hz. *IEEE J. Oceanic Eng.*, **34**, 315–322, doi:10.1109/JOE.2009.2021237.

——, A. A. Cimatoribus, and L. Gostiaux, 2015: Where large deep-ocean waves break. *Geophys. Res. Lett.*, **42**, 2351–2357, doi:10.1002/2015GL063329.